Title	Catchment-scale distribution of radiocesium air dose rate in a mountainous deciduous forest and its relation to topography
Author(s)	Atarashi-Andoh Mariko, Koarashi Jun, Takeuchi Erina, Tsuzuki Katsunori, Nishimura Shusaku, Matsunaga Takeshi
Citation	Journal of Environmental Radioactivity, 147, p.1-7
Text Version	Author's Post-print
URL	https://jopss.jaea.go.jp/search/servlet/search?5049445
DOI	https://doi.org/10.1016/j.jenvrad.2015.05.004
Right	© 2015. This manuscript version is made available under the CC-BY-NC-ND 4.0 license http://creativecommons.org/licenses/by-nc-nd/4.0/

Catchment-scale distribution of radiocesium air dose rate in a mountainous deciduous forest and its relation to topography

Author list and affiliations

Mariko Atarashi-Andoh*, Jun Koarashi, Erina Takeuchi, Katsunori Tsuduki, Syusaku Nishimura, Takeshi Matsunaga

Nuclear Science and Engineering Center, Japan Atomic Energy Agency, Ibaraki 319-1195, Japan.

***Corresponding author**

Tel.: +81 29 282 6860; fax: +81 29 282 6760.

E-mail address: andoh.mariko@jaea.go.jp (M. Atarashi-Andoh).

Highlights (3 to 5 bullet points, maximum 85 characters per bullet point)

- Spatial variation in air dose rates in a mountainous area was investigated
- Measurements obtained by KURAMA-II, NaI detectors, and airborne surveys were compared
- Radiocesium deposition was greater on ridges than in valley bottoms
- Elevation and slope aspect strongly affected air dose rates

Catchment-scale distribution of radiocesium air dose rate in a mountainous deciduous forest and its relation to topography

Abstract

A large number of air dose rate measurements were collected by walking through a mountainous area with a small gamma-ray survey system, KURAMA-II. The data were used to map the air dose rate of a mountainous deciduous forest that received radiocesium from the Fukushima Dai-ichi Nuclear Power Plant accident. Measurements were conducted in a small stream catchment (0.6 km^2 in area) in August and September 2013, and the relationship between air dose rates and the mountainous topography was examined. Air dose rates increased with elevation, indicating that more radiocesium was deposited on ridges, and suggesting that it had remained there for 2.5 y with no significant downslope migration by soil erosion or water drainage. Orientation in relation to the dominant winds when the radioactive plume flowed to the catchment also strongly affected the air dose rates. Based on our continuous measurements using the KURAMA-II, we describe the variation in air dose rates in a mountainous forest area and suggest that it is important to consider topography when determining sampling points and resolution to assess the spatial variability of dose rates and contaminant deposition.

Key words

Air dose rate, Mountainous forest area, KURAMA-II, Fukushima Dai-ichi NPP

accident, Radiocesium deposition

1. Introduction

Most of the area contaminated by radioactive matter from the Fukushima Dai-ichi Nuclear Power Plant (FDNPP) accident is mountainous and forested (~70%) (Hashimoto et al., 2012). Understanding the variation in air dose rates in such areas is essential for effective management of dose exposure for nearby residents and forest workers. It is also important to consider levels of contamination in the context that forests provide recreation and wild food products. Air dose rate and radionuclide deposition mapping has been mainly implemented for residential areas within the 100 km zone of the FDNPP since the accident (Mikami et al., 2015a and 2015b; Saito, 2014; Saito and Onda, 2015; Saito et al., 2015). Airborne monitoring using aircraft has also been conducted in the zone including mountainous forests (Nuclear Regulation Authority, Japan, 2013; Sanada et al., 2013 and 2014). In addition, detailed studies have investigated radiocesium (^{137}Cs and ^{134}Cs) deposition and migration processes on a small spatial scale within forests (e.g., Kato et al., 2012; Koarashi et al., 2012a and 2012b; Matsunaga et al, 2013). However, few studies have assessed the spatial distribution of radiocesium on a catchment scale in extensive mountainous forest areas affected by the FDNPP accident.

Studies that have examined global fallout from nuclear weapons tests and fallout from the Chernobyl NPP accident have indicated that ^{137}Cs distributions in alpine regions are highly heterogeneous because of the complex topography (Albers et al., 1998; Agnesod et al., 2001; Machart et al., 2007; Schaub et al., 2010). Schaub et al. (2010) compared *in situ* soil measurements in the field (using a NaI scintillation detector) with soil measurements in the laboratory (using a GeLi detector) and concluded that the use of small NaI detectors is effective for estimating ^{137}Cs concentration in soil in steep alpine terrain with limited accessibility. Plamboeck et al. (2006) mapped the distribution of ^{137}Cs in a boreal forest using a portable NaI detector connected to a Global Positioning System (GPS) and demonstrated that the detector system has potential for evaluating ^{137}Cs inventories and detecting anomalies over large areas.

In the present study, we evaluated the catchment-scale distribution of radiocesium air dose rates in a mountainous deciduous forest contaminated by the FDNPP accident and its relation to topography. To achieve this, we employed two field measurement methods: (1) continuous measurement while walking through a mountainous area with a KURAMA-II, a system consisting of a small highly sensitive CsI(Tl) scintillation detector and a GPS device, which was originally developed for car-borne radiation surveys (Andoh et al., 2015; Tsuda et al., 2015), and (2) grid-based systematic measurement with a NaI survey meter. Geostatistical analysis was performed on the measurement data to assess the spatial structure of the air dose rate, which allowed us to estimate values at locations where no measurements were carried out and consequently to produce a map for the catchment-scale distribution of air dose rate (Mabit and Bernard, 2007). In addition, the air dose rate data measured by the two methods were compared to each other and to the airborne monitoring data previously reported for the catchment to assess the effectiveness of the methods.

2. Materials and methods

2.1. Study area

This study was conducted in the catchment area of a mountain stream (36.93°N, 140.58°E) in Ibaraki Prefecture, Japan. The site is located ~70 km southwest of the FDNPP and was affected by radioactive fallout from the FDNPP accident at a level of 10–60 kBq m^{-2} of ^{137}Cs deposition according to an airborne monitoring survey (Ministry of Education, Culture, Sports, Science, and Technology, Japan). Several studies have been conducted in the catchment since the accident: ^{137}Cs vertical migration in soil by seepage water (Nakanishi et al., 2014), fluvial discharge of ^{137}Cs via the stream (Matsunaga et al., 2014), and the effects of topography on the redistribution of ^{137}Cs on the forest floor (Koarashi et al., 2014). Furukawa and Shingaki (2012) reported that the gannma radiation dose rate before the FDNPP accident around this study site was 40–50 nGy h^{-1}.

The catchment is located in a temperate forest, dominated by broad-leaved deciduous trees such as Japanese beech (*Fagus crenata*) and Japanese oak (*Quercus serrata*). The trees were leafless in March 2011 when the FDNPP accident occurred. The forest catchment covers an area of 0.6 km^2 with an elevation ranging from 588 to 724 m (Abe et al., 2011). The mean slope angle is 16.5° (range: 0–40°). The mountain stream, which flows into the Shitoki River and belongs to the Same River Basin, flows through the catchment area from northwest to southeast. The mean annual temperature and precipitation are 10.7°C and 1910 mm, respectively (Mizoguchi et al., 2002).

2.2. Air dose rate measurements

2.2.1. Grid-based systematic measurement with a NaI survey meter

The catchment was divided into 150 m (north–south) × 120 m (east–west) rectangular grids, and air dose rates were measured at roughly the center of each of the grids, using a NaI survey meter (TCS-172B, Hitachi-Aloka Medical, Ltd., Tokyo, Japan). The NaI survey meter and the CsI(Tl) scintillation detector incorporated into the KURAMA-II (see the next subsection 2.2.2) are able to accurately measure the ambient dose equivalent rates even if the photon spectrum varies, by utilizing a spectrum-dose conversion function (G[E] function) (Tsuda et al., 2015; Saito et al., 2015). In this paper the obtained value is represented as the "air dose rate". There were 42 measurement points in total: 41 inside the catchment and 1 outside the catchment. The air dose rates were measured at heights of 0.05 m and 1 m. It took 6 d (August 1, 2, 7 and 8, and September 8 and 10, 2013) to complete the measurements.

2.2.2. Continuous measurement while walking with a KURAMA-II system

The KURAMA-II system (Hamamatsu Photonics K.K., Tokyo, Japan) is a GPS-aided mobile radiation monitoring system developed by the Kyoto University Research Reactor Institute (KURRI). Details are reported in Andoh et al. (2015) and Tsuda et al. (2015). For the grid-based systematic measurements, a researcher carried the KURAMA-II unit on a backpack frame while walking through the mountainous area. The CsI(Tl) scintillation detector was set to ~1 m above the ground, collecting air dose rate data and the corresponding GPS locations every 3 s. The statistical error in the air dose rate measurements was ~20% of the background level (< 0.1 μSv h^{-1}) (Tsuda et al., 2015). The shielding effect due to the case, backpack frame, and the carrier's body was confirmed to be negligible by comparison of data collected with and without the shields.

After collecting the data, we extracted 3797 data points for analysis in the following ways: (1) after retaining the first value collected, all extra data collected at the same latitude and longitude were excluded, and (2) the catchment was divided into 5 m grid squares, and the value nearest to the center of each grid was selected as a representative data value for that grid.

2.3. Geostatistical analysis

2.3.1. Topography

Elevation data from the 50 m mesh numerical topographic map published by the Geospatial Information Authority of Japan were used to design a contour map of the catchment and to calculate the slope aspect (octas) and angle of each 10 m square grid. We created a 2D contour map and a 3D surface map using Surfer® 12 (Golden Software, Inc., Golden, CO, USA). The 3D surface map is lit from the east to visualize the relationship between aspect and air dose rates (see Results).

2.3.2. Distribution of air dose rates

Based on the KURAMA-II data, we used the Kriging method to extrapolate air dose rates in new locations within the catchment (Mabit and Bernard, 2007). An experimental variogram (or semi-variogram) was used in an autocorrelation analysis to evaluate the spatial dependence of the values. The variogram $\{\gamma(h)\}$ is a function of separation distance (lag distance, h):

$$\gamma(h)=\frac{1}{2N(h)}\sum_{i=1}^{N(h)}\{Z(x_i)-Z(x_i+h)\}^2 \qquad (1)$$

where $N(h)$ is the number of pairs of observations separated by a distance h, and $Z(x_i)$ and $Z(x_i+h)$ are the measured values at points x_i and x_i+h. The model best fitted to the variograms was used with the Kriging method. The variogram analysis and resulting contour map with Kriging were conducted using Surfer® 12.

3. Results

3.1. Spatial distribution of air dose rates

Figure 1(a) shows a 2D contour map of the study area, and Fig. 1 (b) and 1(c) show the spatial distributions of air dose rates measured by the NaI survey meter (at a height of 1 m above the ground) and KURAMA-II, respectively. Both values obtained at the same measurement points were similar. The western area of the catchment across the river generally had higher air dose rates than the eastern area. Table 1 shows the air dose rates measured by the NaI survey meter (1 m height) and KURAMA-II, which were 0.12–0.52 (mean ± SD, 0.22 ± 0.08) μSv h^{-1} and 0.06–0.59 (0.19 ± 0.07) μSv h^{-1}, respectively.

Figure 2 shows box plots of air dose rates measured using the KURAMA-II within each of the 150 m × 120 m rectangular grids, as well as NaI survey data. The air dose rates varied widely in each grid. The NaI values deviated from the interquartile ranges

(25th to 75th percentile) of KURAMA-II data for more than half of the grids (23 out of 41). The NaI survey data taken at heights of 1 m and 0.05 m showed a linear relationship (Fig. 3, correlation coefficient $r = 0.84$, $p < 0.001$, $n = 41$).

3.2. Relationship between air dose rates and topography

Figure 4 shows dot plots of air dose rates measured by KURAMA-II for each octas slope aspect. Higher values were obtained for northeast-, east-, and southeast-facing slopes, indicating that ^{137}Cs contamination in this area was brought about by wind and rain from the east. Air dose rates increased with elevation ($r = 0.46$, $p < 0.01$) but did not display any clear relationship to slope angles.

Figure 5(a) and 5(b) show the distributions of air dose rates measured along two topographical transects (see also Fig. 1(a) for the locations of the transects in the catchment). The first transect (T1) was ~134 m long from east to west around a ridge, and the air dose rates obtained in a 45-m-wide area (from north to south) across the transect are plotted in Fig. 5(a). This figure demonstrates a large difference in the air dose rate between the east and west sides of the ridge, being higher (on average 0.5 μSv h^{-1}) on the east side and lower (0.2 μSv h^{-1}) on the west side. The west side of the ridge is a Japanese cedar forest and lies outside of the catchment. The second transect (T2) was ~547 m long across the catchment from east to west, and the air dose rates obtained in a 111 m wide area are plotted in Fig. 5(b). The air dose rate increased with elevation on the east-facing slope (the left side of the valley in the figure). In contrast, the air dose rates on the west-facing slope were independent of elevation and generally lower than those on the east-facing slope. Air dose rates were lower on the ridge at the west end (the left end in the figure) than on a slightly lower part of the slope. This is likely because gamma rays observed on the ridge top also originated from the west side of the ridge (outside of the catchment) where there was probably less radiocesium deposition and the air dose rates contained contributions from both aspects.

3.3. Geostatistical analysis

As described above, the air dose rate distribution was affected by elevation and aspect, implying that it is anisotropic. The differences in air dose rates among neighboring points were smaller along the parallel direction to the watercourse (from northwest to southeast) than on the cross direction where the elevation changes steeply (Fig. 1). We conducted a geostatistical analysis using Surfer® 12 taking this anisotropy into consideration (details are given in Golden Software, Inc., Variogram tutorial). The variogram fitted the exponential model well (Fig. 6). The nugget-to-sill (nugget + scale) ratio was 22.2%, indicating that air dose rate has a strong spatial dependence (Cambardella et al., 1994; Mabit and Bernard, 2007). Figure 7(a) shows a 3D contour map of the study area, and Fig. 7(b) shows the contours of the air dose rates in the catchment, which were drawn based on the results of the geostatistical analysis.

4. Discussion

4.1. Catchment-scale distribution of air dose rates and its relation to topography

The results obtained with the two field methods (the grid-based systematic measurement and continuous measurement) showed that the air dose rates in the mountainous forested area are highly spatially variable and topographically anisotropic (Figs. 1 and 2). The air dose rates measured at 0.05 m by the NaI survey meter are mainly due to gamma rays from the soil, while those measured at 1 m are considered to contain gamma rays from the surrounding area within a ~60 m radius (both soil and tree canopy) (Andoh et al., 2015). However, a strong linear relationship was found between the air dose rates from the two methods (Fig. 3), indicating a predominant contribution of soil radiocesium to the air dose rates at 1 m height (where the air dose rates were also measured by the KURAMA-II). A few outliers can be found in Figure 3, which may be due to high spatial variation in radiocesium deposition to the soil even over a small area (Schaub et al., 2010). Another potential cause for the outliers is a larger contribution of gamma rays from tree canopies at the measurement points. However, the vegetation at this site consists of deciduous trees; it is likely that almost all of the radiocesium existed on the soil surface at the time of investigation (roughly 2.5 y after the accident). After the Chernobyl NPP accident, tree canopy contamination fell rapidly over a period of weeks or months, and ^{137}Cs stored in the forest standing biomass was only ~5% of the total activity in a forest ecosystem (IAEA, 2006). Thus, gamma rays from tree canopies were likely not a factor. The predominant contribution of soil radiocesium to the air dose rates at 1 m height suggests that these air dose rates can possibly be used to evaluate the deposition density of radiocesium on soil at this site. Nakanishi et al. (2014) reported that the total inventory of ^{137}Cs (in litter and 0–10 cm soil depth) at a point in this study area was ~22 kBq m^{-2} on 23 August 2012. The air dose rate measured using the KURAMA-II was 0.17 μSv h^{-1} at the same point. Assuming that the background air dose rate without accidental ^{137}Cs deposition was 0.045 μSv h^{-1} (Furukawa and Shingaki, 2012), the ratio of ^{137}Cs deposition density to air dose rate was calculated as 176. However, more ^{137}Cs deposition density data are necessary to accurately determine the ratio.

Although it is well-documented that the structure of the forest canopy is important in determining the extent of fallout-^{137}Cs interception (Bunzl et al., 1989; Nimis, 1996), our results clearly demonstrate that the elevation and slope aspect are also very important. We found a well-defined proportional relationship between the air dose rate and elevation on the east-facing slope {Fig. 5(b)}. Schaub et al. (2010) observed a similar relationship in an alpine site. The effect of aspect may further complicate the relationship between air dose rate and elevation. The spatial pattern of the air dose rate was similar to the lighting pattern in the 3D surface map (Fig. 7), indicating that radiocesium deposition is strongly affected by an east wind in this catchment. It is reasonable to assume that aerosol interception by mountainous forests is greater for dry deposition than for wet deposition because radiocesium in raindrops should uniformly reach the soil surface over the catchment, although radiocesium distribution is affected by rain intensity (Nimis, 1996). According to a numerical simulation by Terada et al. (2012), deposition after the FDNPP accident was mainly due to dry deposition at our study site, and dry deposition was estimated to account for 60–80% of the total deposition. To understand the general relationship between air dose rate and elevation, more investigations on the distribution of air dose rates on a catchment scale are necessary under varying deposition conditions, and the present study presents a useful method for this purpose.

Radiocesium deposited on soil binds to soil particles (Sawhney, 1972), and therefore soil erosion is an important factor in migration of ^{137}Cs on slopes (e.g., Bonnett, 1990; Fukuyama et al., 2005). Leaf litter on forest soil also retains some radiocesium, such that migration with leaf litter caused by wind is also possible. On a steep slope at our study site, Koarashi et al. (2014) reported that ^{137}Cs accumulation in the litter layer at the bottom of the slope was five-fold higher than that at 12 m above the bottom, which is rapidly driven by biologically mediated processes. Our large-scale (ranging from hundreds to thousands of meters) investigation on air dose rates, however, showed that most radiocesium remained on the ridges on the catchment scale; this can be largely explained by the larger deposition of Fukushima-derived radiocesium in higher-elevation areas. Therefore, the topographically biased distribution pattern of radiocesium in the catchment suggests that a slowed fluvial discharge of radiocesium from the forest via the stream is possible despite the fact that the forest is located in a mountainous and hilly region with steep terrain. Our measurements were taken ~2.5 y after the accident, and it is therefore unclear how radiocesium deposited to soil had migrated along slopes over this period. Additional studies on the spatial distribution of air dose rate using the KURAMA-II at the same site are required to estimate future migration patterns.

4.2. Comparison of the two methods

The two methods yielded similar statistical results for air dose rates (Table 1). However, the high spatial variation in air dose rate even in the 150 m × 120 m grids (Fig. 2) indicates that continuous measurements using the KURAMA-II is more effective for estimating accurate distributions over a large area. The limited number of measurements carries the risk of over- or underestimation if the measurement points are not selected carefully. Moreover, using geostatistical analysis, the air dose rate was interpolated successfully when taking topographical anisotropy into consideration, which was determined based on the continuous measurements. The contour map {Fig. 7(b)} shows the spatial variation in air dose rate. This will be important for developing radiation dose management strategies for nearby residents and forest workers. The data can also be used to evaluate the deposition density of radiocesium on soil (see section 4.1). The results of the comparison of the two methods suggest that grid size and measurement points should be carefully determined by considering the topographic features of the target (catchment-scale) area when grid-based systematic measurements are used.

4.3. Comparison with airborne monitoring

The Nuclear Regulation Authority in Japan has monitored air dose rates based on a series of aircraft surveys. The seventh airborne monitoring was performed in September 2013; the average air dose rate for the catchment area was 0.20 μSv h^{-1} (range: 0.18–0.21 μSv h^{-1}), similar to our results (0.22 ± 0.08 μSv h^{-1} and 0.19 ± 0.07 μSv h^{-1} for the grid-based systematic and continuous measurements, respectively; see Table 1). This implies that airborne monitoring provides an accurate estimation of the air dose rate averaged over thousands of meters even in mountainous areas. However, the spatial variation in the air dose rate in the catchment revealed by our field measurements was not identified from the airborne results.

5. Conclusion

We evaluated the spatial distribution of radiocesium air dose rates in a mountainous deciduous forest contaminated by the FDNPP accident, and estimated the relationship between air dose rate and topographical features by continuous measurements using the KURAMA-II system. Air dose rates were highly spatially variable and topographically anisotropic. There was a well-defined proportional relationship between air dose rate and elevation on the east-facing slope. However, the air dose rate on the opposite slope was independent of elevation. We conducted a geostatistical analysis taking this anisotropy into consideration. The resulting contour map revealed a larger inventory of radiocesium on the ridge 2.5 y after the deposition, mainly due to a larger deposition density. Further investigation using a KURAMA-II at the same site will be useful for evaluating the long-term catchment-scale migration of radiocesium in the mountainous forest area. The present study was conducted in a deciduous broad-leaved forest where dry deposition was dominant after the FDNPP accident. Therefore, further studies in mountainous forest areas under varying deposition and vegetation conditions using the same methods employed in the present study will aid understanding of the relationship between air dose rate and topography.

Acknowledgments

The authors thank the Ibaraki District Forest Office for permission to use the Ogawa Forest Reserve site. The authors also thank K. Saito and M. Andoh of the Fukushima Environmental Safety Center, Japan Atomic Energy Agency (JAEA) for their support with the KURAMA-II measurements, and M. Ishihara and K. Matsumura of the JAEA for support with organizing the field data.

References

Abe, T., Fujieda, M., Kabeya, N., Kubota, T., Noguchi, H., Shimizu, A., Tsuboyama, Y., Noguchi, S., 2011. Report of hydrological observations at the Ogawa Forest Reserve (August 2000 to September 2007). Bulletin of FFPRI **10**(4), 291–317 (in Japanese with English abstract).

Agnesod, G., Lazzaron, R., Operti, C., Zappa, C., 2001. Accuracy of field spectrometry in estimating ^{137}Cs contamination in high altitude alpine soils. Radiat. Prot. Dosim., **97**(4), 329-332.

Albers, B.P., Rackwitz, R., Schimmack, W., Bunzl, K., 1998. Transect survey of radiocesium in soils and plants of two alpine pastures. Sci. Total Environ., **216**, 159–172.

Andoh, M., Nakahara, Y., Tsuda, S., Yoshida, T., Matsuda, N., Takahashi, F., Mikami, S., Kinouchi, N., Sato, T., Tanigaki, M., Takamiya, K., Sato, N., Okumura, R., Uchihori, Y., Saito, K., 2015. Measurement of air dose rates over a wide area around the Fukushima Dai-ichi Nuclear Power Plant through a series of car-borne surveys. J. Environ. Radioact., **139**, 266–280.

Bonnett, P. J. P., 1990. A review of the erosional behaviour of radionuclides in selected drainage basins. J. Environ. Radioact., **11**, 251–266.

Bunzl, K., Schimmack, W., Kreutzer, K., Schierl, R., 1989. Interception and retention of Chernobyl-derived ^{134}Cs, ^{137}Cs and ^{106}Ru in a spruce stand. Sci. Total Environ., **78**, 77–87.

Cambardella, C. A., Moorman, T. B., Novak, J. M., Parkin, T. B., Karlen, D. L., Turco,

R. F., Konopka, A. E., 1994. Field-scale variability of soil properties in central Iowa soils. Soil Sci. Soc. Am. J., **58**, 1501–1511.

Fukuyama, T., Takenaka, C., Onda, Y., 2005. ^{137}Cs loss via soil erosion from a mountainous headwater catchment in central Japan. Sci. Total Environ., **350**, 238–247.

Furukawa, M., Shingaki, R., 2012. Terrestrial gamma radiation dose rate in Japan estimated before the 2011 Great East Japan Earthquake. Radiat. Emerg. Med., **1**, 11–16

Golden Software, Inc., 2014. Surfer® 12 Full User's Guide, Colorado, USA. Golden software, Inc.. Variogram tutorial, http://www.goldensoftware.com/variogramTutorial.pdf (accessed 2014.10.21)

Hashimoto, S., Ugawa, S., Nanko, K. & Shichi, K., 2012. The total amounts of radioactively contaminated materials in forests in Fukushima Japan. Sci. Rep., **2**, 416, DOI: 10.1038/srep00416.

International Atomic Energy Agency (IAEA), 2006. Environmental Consequences of the Chernobyl Accident and their Remediation: Twenty Years of Experience. Vienna, IAEA.

Kato, H., Onda, Y., Gomi, T., 2012 Interception of the Fukushima reactor accident-derived ^{137}Cs, ^{134}Cs and ^{131}I by coniferous forest canopies. Geophys. Res. Lett., **39**(20), DOI: 10.1029/2012GL052928.

Koarashi, J., Atarashi-Andoh, M., Matsunaga, T., Sato, T., Nagao, S., Nagai, H., 2012a. Factors affecting vertical distribution of Fukushima accident-derived radiocesium in soil under different land-use conditions. Sci. Total Environ., **431**, 392–401.

Koarashi, J., Moriya, K., Atarashi-Andoh, M., Matsunaga, T., Fujita, H., Nagaoka, M., 2012b. Retention of potentially mobile radiocesium in forest surface soils affected by the Fukushima nuclear accident. Sci. Rep., **2**, 1005, DOI:10.1038/srep01005.

Koarashi, J., Atarashi-Andoh, M., Takeuchi, E., Nishimura, S., 2014. Topographic heterogeneity effect on the accumulation of Fukushima-derived radiocesium on forest floor driven by biologically mediated processes. Sci. Rep., **4**, 6853, DOI:10.1038/srep06853.

Mabit, L., Bernard, C., 2007. Assessment of spatial distribution of fallout radionuclides through geostatistics concept. J. Environ. Radioact., **97**, 206–219.

Machart, P., Hofmann, W., Türk, R., Steger, F., 2007. Ecological half-life of ^{137}Cs in lichens in an alpine region. J. Environ. Radioact., **97**, 70–75.

Matsunaga, T., Koarashi, J., Atarashi-Andoh, M., Nagao, S., Sato, T., Nagai, H., 2013. Comparison of the vertical distributions of Fukushima nuclear accident radiocesium in soil before and after the first rainy season, with physicochemical and mineralogical interpretations. Sci. Total Environ., **447**, 301–314.

Matsunaga, T., Nakanishi, T., Atarashi-Andoh, M., Takeuchi, E., Tsuduki, K., Nishimura, S., Koarashi, J., Otosaka, S., Sato, T., Nagao, S., 2014. A passive collection system for whole size fractions in river suspended solids. J. Radioanal. Nucl. Chem., DOI:.1007/s10967-014-3491-5.

Mikami, S., Maeyama, T., Hoshide, Y., Sakamoto, R., Sato, S., Okuda, N., Sato, T., Takemiya, H., Saito, K., 2015a. The air dose rate around the Fukushima Dai-ichi

Nuclear Power Plant: its spatial characteristics and temporal changes until December 2012. J. Environ. Radioact., **139**, 250–259.

Mikami, S., Maeyama, T., Hoshide, Y., Sakamoto, R., Sato, S., Okuda, N., Demongeot, S., Gurriaran, R., Uwamino, Y., Kato, H., Fujiwara, M., Sato, T., Takemiya, H., Saito, K., 2015b. Spatial distributions of radionuclides deposited onto ground soil around the Fukushima Dai-ichi Nuclear Power Plant and their temporal change until December 2012. J. Environ. Radioact, **139**, 320–343

Ministry of Education, Culture, Sports, Science, and Technology, Japan. Preparation of Distribution Map of Radiation Doses, etc. (Map of Radioactive Cesium Concentration in Soil) by MEXT. http://radioactivity.nsr.go.jp/en/contents/5000/4165/24/1750_083014.pdf (accessed 2014.6.7).

Ministry of Education, Culture, Sports, Science, and Technology, Japan. Extension Site of Distribution Map of Radiation Dose, etc. http://ramap.jmc.or.jp/map/eng/ (accessed 2014.6.13).

Mizoguchi, Y., Morisawa, T., Ohtani, Y., 2002. Climate in Ogawa Forest Reserve. In: Nakashizuka, T., Matsumoto, Y. (Eds.) Ecological Studies, **158**, 11–18, Diversity and Interaction in a Temperate Forest Community: Ogawa Forest Reserve of Japan, Springer-Verlag, Tokyo.

Nakanishi, T., Matsunaga, T., Koarashi, J., Atarashi-Andoh, M., 2014. ^{137}Cs vertical migration in a deciduous forest soil following the Fukushima Dai-ichi Nuclear Power Plant accident. J. Environ. Radioact., **128**, 9–14.

Ninmis, P. L., 1996. Radiocesium in plants of forest ecosystems. Studia Geobotanica., **15**, 3–49.

Nuclear Regulation Authority, Japan, 2013. Monitoring information of environmental radioactivity level, http://radioactivity.nsr.go.jp/en/list/307/list-1.html (accessed at 2014.10.15).

Plamboeck, A. H., Nylén, T., Ågren, G., 2006. Comparative estimations of ^{137}Cs distribution in a boreal forest in northern Sweden using a traditional sampling approach and a portable NaI detector. J. Environ. Radioact., **90**, 100–109.

Saito, K., 2014. Mapping and modeling of radionuclide distribution on the ground due to the Fukushima accident. Radiat. Prot. Dosim., doi:10.1093/rpd/ncu011.

Saito, K., Onda, Y., 2015. Outline of the national mapping projects implemented after the Fukushima accident. J. Environ. Radioact., **139**, 240–249.

Saito, K., Tanihata, I., Fujiwara, M., Saito, T., Shimoura, S., Otsuka, T., Onda, Y., Hoshi, M., Ikeuchi, Y., Takahashi, F., Kinouchi, N., Saegusa, J., Seki, A., Takemiya, H., Shibata, T., 2015. Detailed deposition density maps constructed by large-scale soil sampling for gamma-ray emitting radioactive nuclides from the Fukushima Dai-ichi Nuclear Power Plant accident. J. Environ. Radioact., **139**, 308–319.

Sanada, Y., Kondo, A., Sugita, T., Nishizawa, Y., Yuuki, Y., Ikeda, K., Shoji, Y., Torii, T., 2013. Radiation monitoring using an unmanned helicopter in the evacuation zone around the Fukushima Daiichi nuclear power plant. Explor. Geophys., **45**, 3–7.

Sanada, Y., Sugita, T., Nishizawa, Y., Kondo, A., Torii, T.,2014. The aerial radiation monitoring in Japan after the Fukushima Daiichi nuclear power plant accident. Prog.

Nucl. Sci. Technol., **4**, 76–80.

Sawhney, B. L., 1972. Selective sorption and fixation of cations by clay minerals: a review. Clay Clay Miner., **20**, 93–100.

Schaub, M., Konz, N., Meusburger, K., Alewell, C., 2010. Application of in-situ measurement to determine ^{137}Cs in the Swiss Alps. J. Environ. Radioact., **101**, 369–376.

Terada, H., Katata, G., Chino, M., Nagai, H., 2012. Atmospheric discharge and dispersion of radionuclides during the Fukushima Dai-ichi Nuclear Power Plant accident. Part II: verification of the source term and analysis of regional-scale atmospheric dispersion. J. Environ. Radioact., **112**, 141–154.

Tsuda, S., Yoshida, T., Tsutsumi, M., Saito, K., 2015. Characteristics and verification of a car-borne survey system for dose rates in air: KURAMA-II. J. Environ. Radioact., **139**, 260–265.

Figure captions

Fig. 1. (a) Topographical map of the study site, (b) air dose rates measured by the NaI survey meter, and (c) air dose rates measured by the KURAMA-II system. Black, blue, and red lines (T1 and T2) in Fig. 1(a) show watersheds, streams, and transects used for detailed analysis in Fig. 5, respectively.

Fig. 2. Box plots of air dose rates measured using KURAMA-II for 150 m × 120 m rectangular grids with the NaI measurement points in the grid center. (A) = maximum excluding outliers, (B) = 75th percentile (UQ), (C) = median, (D) = 25th percentile (LQ), (E) = minimum excluding outliers, (F) = outliers { > UQ + 1.5 × (UQ – LQ) or < LQ – 1.5 × (UQ – LQ)}. Black squares show air dose rates measured using the NaI survey meter at 1 m height.

Fig. 3. Scatter plot of air dose rates at heights of 1 m and 0.05 m, measured using the NaI survey meter. The regression line fitted to the plotted data and the correlation coefficient are also shown.

Fig. 4. Dot plots of the air dose rates measured using the KURAMA-II for each slope aspect. The lines in the figure indicate the arithmetic means of air dose rates for each slope aspect.

Fig. 5. Topographical cross-sections and air dose rates for transects T1 (a) and T2 (b). The locations of the transects in the catchment are shown as lines in Fig. 1(a). In the upper graphs, circles, squares, and diamonds represent results from the KURAMA-II, NaI survey meter at 0.05 m, and NaI survey meter at 1 m, respectively.

Fig. 6. Variogram of air dose rates measured using the KURAMA-II system. The line represents an exponential model. Model constants are also shown.

Fig. 7. A 3D surface map of the study site and contour map of the air dose rates. (a) A 3D surface map lit from the east and (b) contour map of the air dose rates in the catchment. The black lines in Fig. 7(a) indicate watersheds. The mountain stream runs from the far to the near side.

Fig. 1 (Atarashi-Andoh et al.) Color in the Web and in print

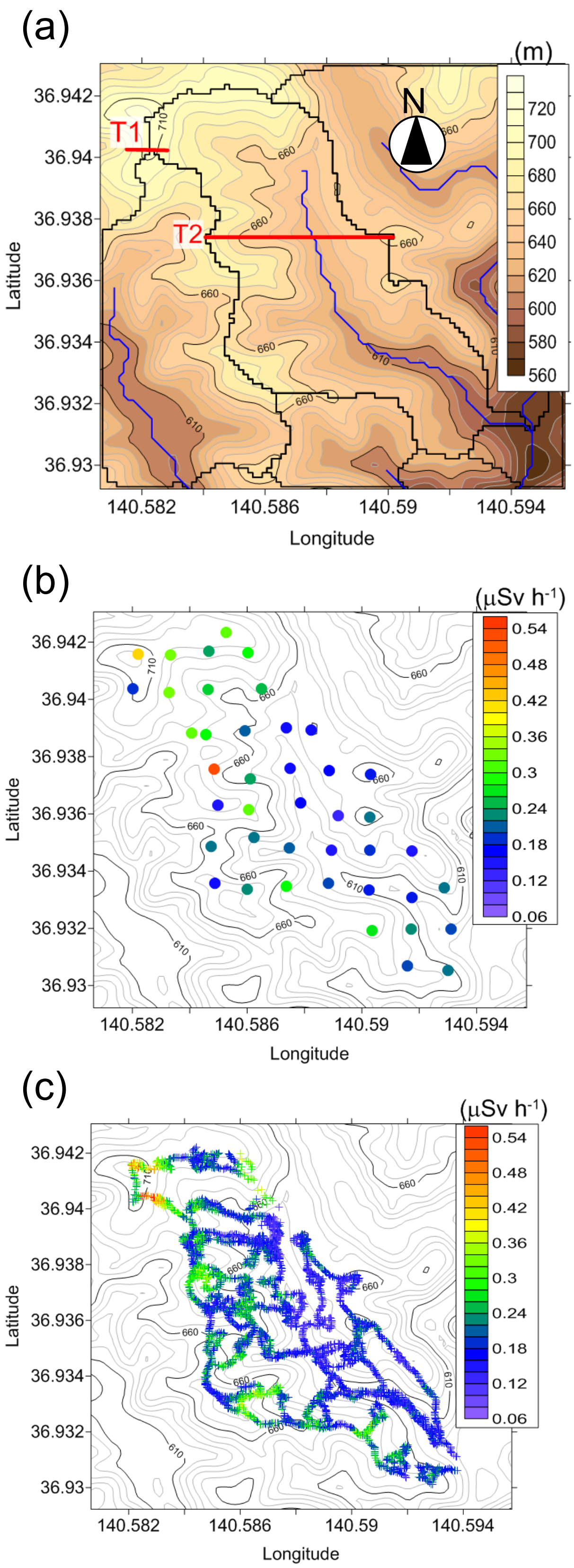

Fig. 2 (Atarashi-Andoh et al.)

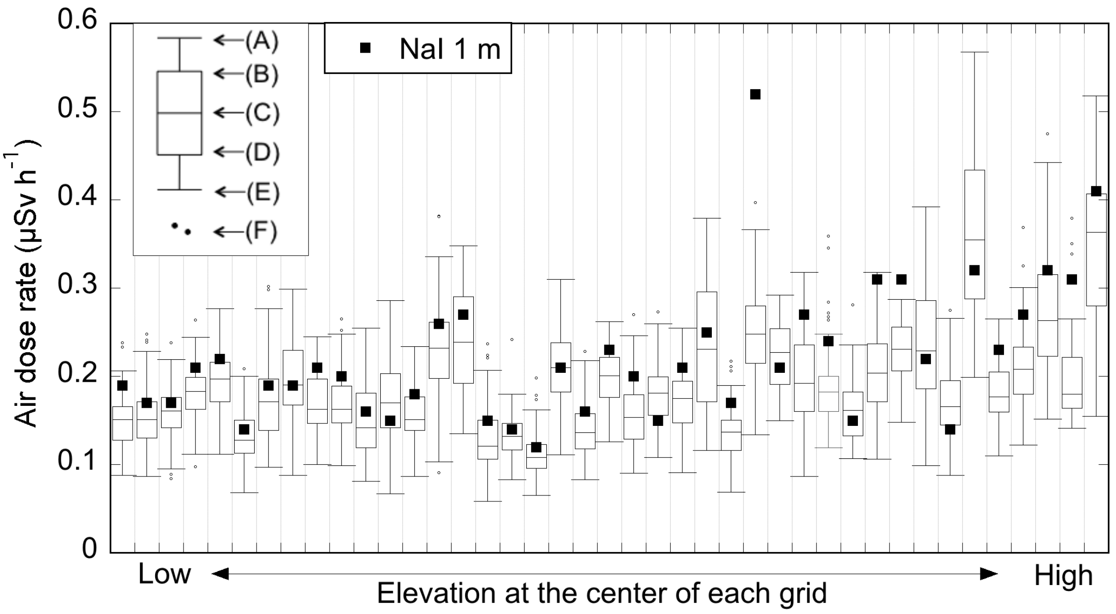

Fig.3 (Atarashi-Andoh et al.)

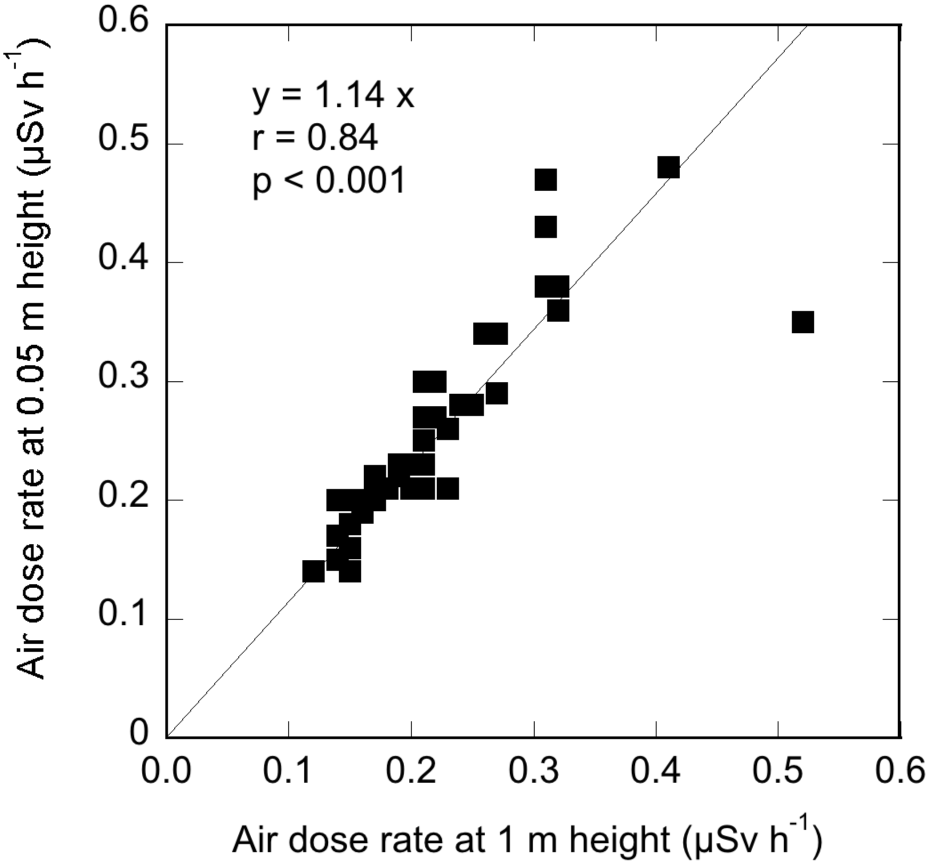

Fig.4 (Atarashi-Andoh et al.)

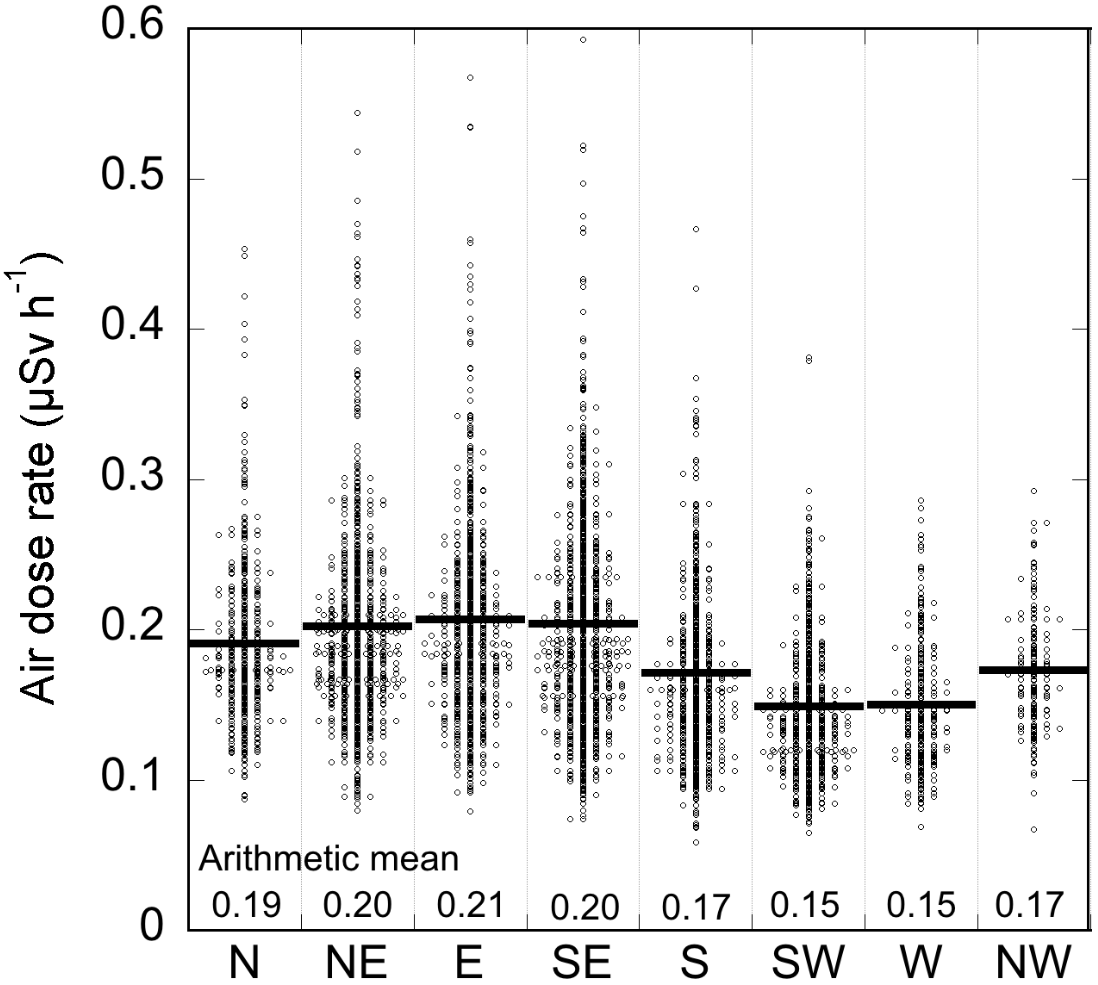

Fig.5 (Atarashi-Andoh et al.)

(a) T1

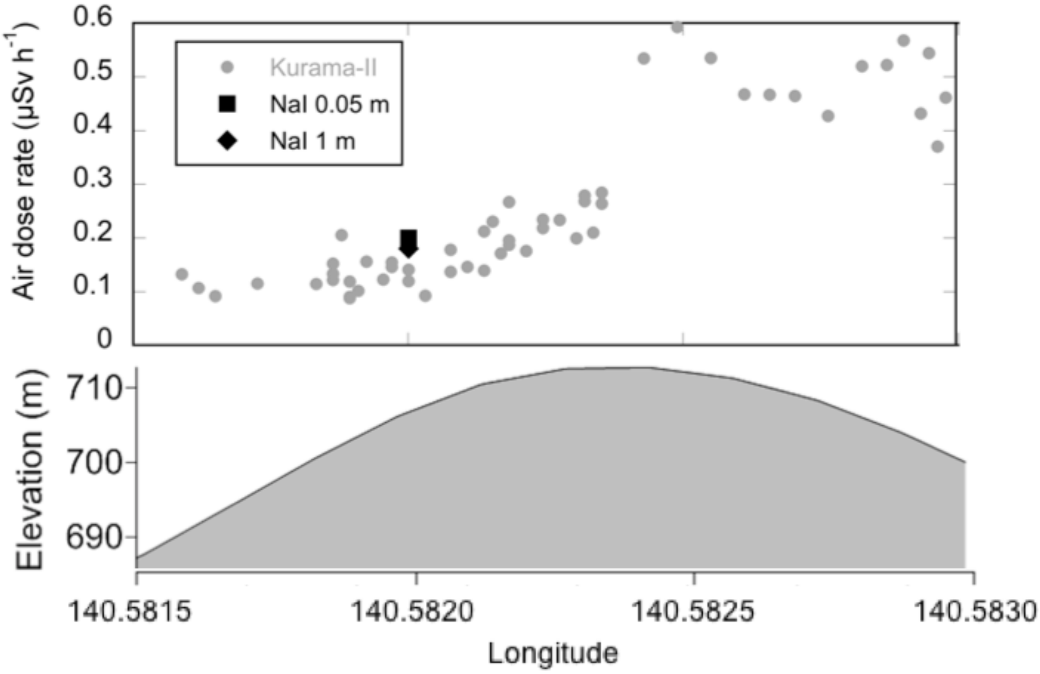

(b) T2

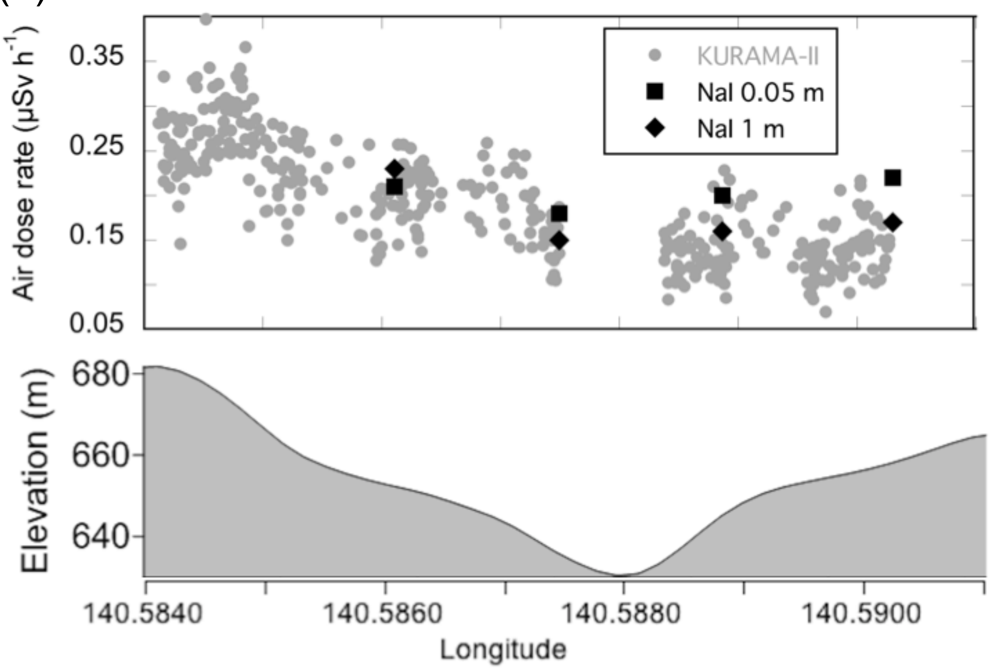

Fig.6 (Atarashi-Andoh et al.)

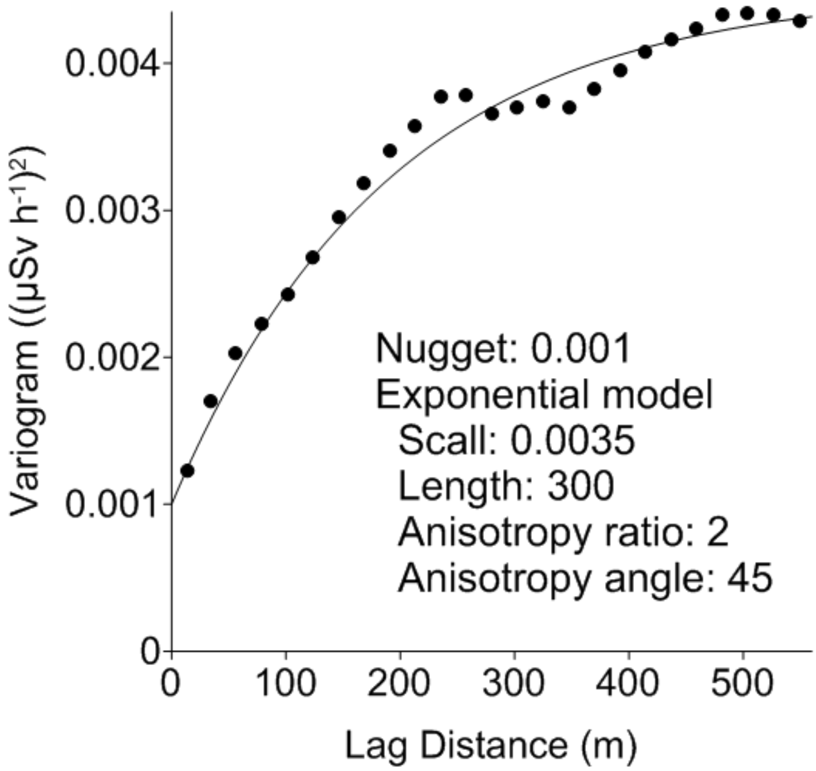

Fig.7 (Atarashi-Andoh et al.) Color in the Web and in print

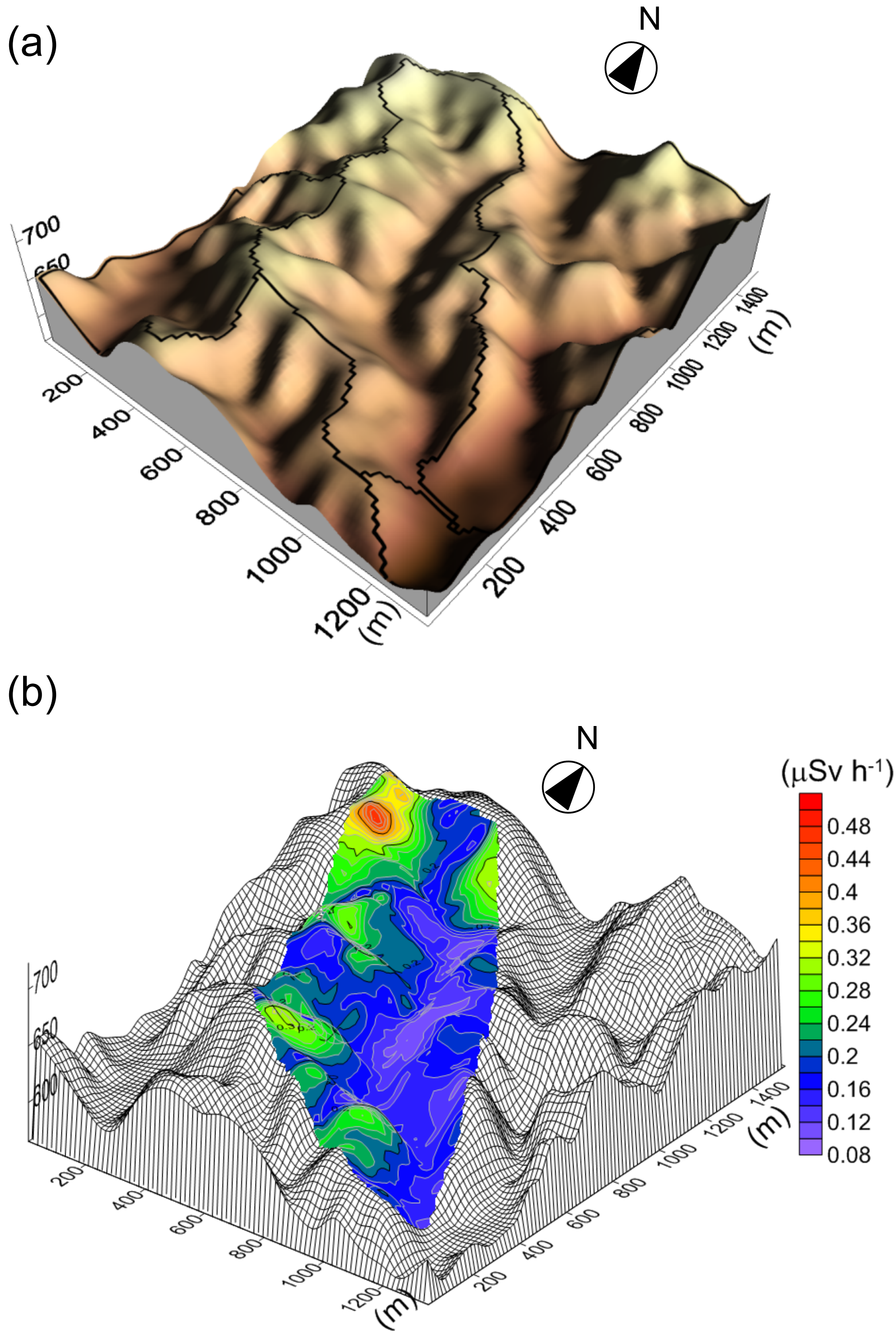

Table 1

Number of data and statistics of air dose rates (μSv h^{-1})

	NaI survey meter[a]	KURAMA-II[a]
Number of data	41	3797
Arithmetic mean	0.22	0.19
SD	0.08	0.07
Maximum	0.52	0.59
Minimum	0.12	0.06
Median	0.21	0.18

[a]Measured at 1 m height